Invited Paper

Photo-Excited Silicon-Based Spatial Terahertz Modulators

Yu-Lian He, Yuan-Sheng Wang, and Qi-Ye Wen *
State Key Laboratory of Electronic Thin Films and Integrated Devices, University of Electronic Science and Technology of China, Chengdu 611731, China
* Email: qywen@uestc.edu.cn

(Received January 4, 2021)

Abstract: The increasing development of terahertz (THz) technology has led to various potential applications in THz imaging, spectroscopy and communications. These devices capable of actively manipulating the amplitude, phase and frequency of THz waves are thus gaining numerous interests. All-optical silicon-based spatial terahertz modulators (STMs), as a simple, cost-effective, and reconfigurable technique, are standing the focus of research. Beginning with a fundamental concept of THz radiation, this paper systematically summarized the modulation mechanism and theoretical model for this kind of STM, reviewed the recent advancements in THz functional devices implemented by this optical method and yet, discussed the performance-improved measures with an emphasis on the reflection reduction. Despite that, there has been considerable progress in realizing high-performance STMs, and novel design is urgent to realize higher modulation rate and more functionality.

Keywords: Terahertz, All optical devices, Manipulation, Spatial modulator, Silicon devices

doi:

1. Introduction

Terahertz (THz) radiation situated between microwave and infrared regions of electromagnetic spectrum has become increasingly attractive for its extraordinary properties. Without a standard definition, THz band is commonly referred as the range of 30 μm to 3 mm in wavelength and 0.1 THz to 10 THz in frequency [1]. This special frequency spectrum motivates THz technology preferably meritorious in numerous sectors spanning from industry, defense, medical to scientific research [2, 3]. Representatives are THz spectroscopy and sensing, THz imaging and near-field microscopy, and THz radar and communications [4, 5]. With the significant advancement of THz source and detection techniques, physical properties of materials, for instance, carrier density calculation, molecular identification and internal structure analysis have been investigated employing THz spectroscopy and sensing [6, 7]. THz image and near-field microscopy is mainly used for nondestructive inspection, medical diagnose as well as security detection. As for THz radar and communications, it is one of the most promising applications especially in the fields of interplanetary communications, short-range atmosphere communications [8] and wireless LAN communications.

Such widespread deployment of THz technology applications has pushed THz research into the center stage. However, its full exploitation remains technically challenging due to the typical natural materials' poor response to THz radiation. The imperious demand for active devices which could manipulate THz radiation efficiently is driving THz modulation a hotspot in THz research. As a fundamental functionality, THz modulation is highly requested to satisfy the demand for fast, high-efficiency, low cost, easy fabrication and integration indeed. Although numerous efforts have been reported with electrical gating or thermal controlling scheme [9, 10], optically controlled THz modulators are increasingly important and in demand, attributing to the strict conditions of material and working ambient in thermal-controlled modulators and the relatively high requirements of materials and processing in electric-controlled ones [9, 11].

Generally, semiconductor materials are employed to fabricate THz optical modulators. When optical illumination is radiated to a semiconductor, free carriers could be generated once its energy ($\hbar\omega$) is larger than that of bandgap (E_g) of semiconductor, i.e., $\hbar\omega \geq E_g$. The photo-induced carriers (electrons or holes) density (N) is proportionally related to the fluence (energy per unit area) of incident photons and commonly described by Drude model,

$$\tilde{\sigma}(\omega) = \varepsilon_0 \frac{\omega_p^2 \tau}{1 - i\omega\tau} \tag{1}$$

where $\tilde{\sigma}(\omega)$ is the complex conductivity and ε_0, τ, m and e are the permittivity of free space, scattering rate, electron mass and electron charge, respectively. ω_p represents the plasma frequency, $\omega_p = \sqrt{Ne^2/\varepsilon_0 m}$, a characteristic frequency below which the material acts "metallic" while above which it is transparent to optical radiation. This phenomenon indicates that semiconductors are suitable for all-optical modulation of THz waves: A high-reflectance region is temporarily formed onto the semiconductor when the laser is incident and thus the co-projected THz radiation on this area is modulated.

Regular semiconductor materials, such as silicon (Si), gallium arsenide (GaAs) and germanium (Ge), have been resoundingly put to use in optical-controlled THz waves modulators [12-19]. Si-based modulators are the priority of implementing THz spatial modulation and have been most investigated. In this paper, we mainly concentrate on the researches of THz spatial modulation by optically excited electron plasma in photo-active Si substrate. Starting with the generating mechanism of photo-carriers, THz wave manipulation by laser illuminating Si wafer is theoretically analyzed in Section 2. Section 3 introduces such modulation scheme based experimental demonstration on functional elements. Corresponding performance enhancement measures are exhibited in Section 4. Finally the outlook is concluded in Section 5.

2. Modulation Mechanism by Photo-Exciting Si

Si, existing in the fourth group in periodic table and possessing a wide bandgap (1.12 *eV*), is one of the best candidates to manage THz radiation. Owing to its indirect bandgap characteristic, laser with a wavelength less than 1107 *nm* can be capable to produce photo-carriers, efficiently controlling free carriers density. Consequently pronounced changes of complex refractive index and hence the optical properties of Si may occur, which makes the transmissivity and reflectivity in the THz range vary. As early as 1983, Salzmann *et al*. utilized 337 *nm* pulsed laser to irradiate high-resistivity Si wafer and realized subnanosecond level of amplitude switching of 119 *μm* radiation in both transmission and reflection [20]. Fekete *et al*. theoretically studied and experimentally demonstrated the validity of light-controllable THz reflectivity of high-resistivity Si wafers under both 405 nm and 810 *nm* illumination [21]. Whereafter, three different wavelengths of 1064 *nm*, 532 *nm* and 355 *nm* were demonstrated in 214 *μm* radiation modulation, the transmitted waves intensity decreased while that of reflected increased when laser-on [22]. The observed change of THz waves transmissivity and reflectivity going through a pulse laser excited high-resistivity Si wafer is caused by the temporal and spatial perturbation of free carriers density. The dynamic behavior of free carriers density yields the dynamics of the complex dielectric constant in the Si wafer. The THz optical properties is thus regulated. Such modulation scheme could be theoretically characterized by using Drude's theory and concluded in three steps: free carriers density formulation, complex refractive index formulation and transmission/reflection formulation.

A. Free carriers density formulation

When an effective illumination ($\lambda \leq 1107$ *nm*) is interacted with Si, the dynamic behavior of free carriers include generation, recombination and diffusion, which could be described by the continuity equation [23-25]:

$$\frac{\partial N(x,z,t)}{\partial t} = G(x,z,t) - R(x,z,t) - \vec{\nabla} \cdot \vec{J} \tag{2}$$

in which x denotes the spatial coordinate parallel to the Si surface while z refers to the direction of the propagating THz beam, that is, perpendicular to Si. The carriers generation rate $G(x,z,t)$ and recombination rate $R(x,z,t)$ are both time- and space-dependent. Since the absorption depth d is much smaller than the dimension of the homogeneously irradiated Si area, it is justified to make a one-dimensional approximation for eq. (2).

Now therefore the carriers generation rate $G(x,z,t)$ can be written as

$$G(z,t) = \frac{(1-R)\alpha I(t)}{\hbar\omega} e^{-\alpha z} \tag{3}$$

which signifies that the free electron-hole carriers are generated at a depth z through band-to-band absorption by a single pulse of intensity $I(t)$ and photon energy $\hbar\omega$ incident on silicon at an angle with a reflectivity R and an absorption coefficient α.

As for the recombination, there mainly exist three components consisting of Auger recombination, radiative recombination and that via lattice imperfections and impurities which are characterized by γ_3, γ_2 and γ_1, respectively. The recombination term $R(x,z,t)$ is thus given as

$$R(z,t) = \gamma_3\left[N(z,t),T\right]N^3(z,t) + \gamma_2 N^2(z,t) + \gamma_1 N(z,t) \tag{4}$$

where γ_1 and γ_2 are constant for a specific Si sample, while $\gamma_3\left[N(z,t),T\right]$ is a function of the induced carriers density $N(z,t)$ and the carrier-lattice temperature T [26].

The $\vec{\nabla}\cdot\vec{J}$ term delineates the coupled diffusion process of a photo-generated electron-hole plasma and the associated lattice-carrier temperature and $\vec{J}$ is termed as the electron-hole current density, written as

$$\vec{J} = -D\left[N(z,t)\right]\left[\vec{\nabla}N(z,t) + \frac{N(z,t)}{2T}(1-r)\vec{\nabla}T\right] \tag{5}$$

with $D\left[N(z,t)\right]$ being the ambipolar diffusivity [27] and $r = -k_B^{-1}\left(\partial E_g/\partial T\right)$.

Assuming a surface recombination occurred on the top surface of Si, the carriers density $N(z,t)$ satisfies the boundary condition:

$$N(z,t)\big|_{z=h} = N_i,\ \ D\left[N(z,t)\right]\cdot\frac{\partial N(z,t)}{\partial z}\bigg|_{z=0} = S\left[N(z,t) - N_i\right] \tag{6}$$

where h is the Si sample thickness, N_i is the intrinsic equilibrium carriers density for Si, and S denotes the surface recombination rate depending on the surface condition.

Because the material parameters such as $\vec{J}$ and γ_3 are lattice-temperature-dependent, heat generation should be considered which is mainly induced by two processes. One is in the laser absorption process, where the excess energy is lost by the electron-hole pairs instantaneously and assumed to be $\hbar\omega - E_g - 2\left(3k_BT/2\right)$. The other occurs via the recombination process where the energy $E_g + 2\left(3k_BT/2\right)$ lost by the recombining electron-hole pairs is transferred immediately to the lattice. The thermal diffusion equation can therefore be described as

$$\frac{\partial T}{\partial t}=\frac{\partial}{\partial z}\left(D_L\frac{\partial T}{\partial z}\right)+\frac{(1-R)I(t)\alpha e^{-\alpha z}}{C}\left(\hbar\omega-E_g-3k_BT\right)$$
$$+\frac{E_g+3k_BT}{C}\left\{\gamma_3\left[N(z,t),T\right]N^3(z,t)+\gamma_2N^2(z,t)+\gamma_1N(z,t)\right\} \tag{7}$$

where C is the specific heat and D_L is the lattice thermal diffusivity, which meets the boundary condition shown in eq. (8) for the reason that little heat is lost from the surface on a nanosecond time scale while the heat is produced at the surface once $S\neq 0$,

$$K_T\frac{\partial T}{\partial z}+S\left[N(z,t)-N_i\right]\left(E_g+3k_BT\right)=0,\quad T\big|_{z=h}=300\text{ K} \tag{8}$$

in which K_T is the thermal conductivity and D_L=K_T/C [28]. For a given laser pulse, for example the sine-square-shaped laser used in [23], the carriers density is thus numerically solved.

B. Complex refractive index formulation

According to Fresnel formula, the transmission of normally incident THz waves through the photo-excited Si wafer is determined by the complex refractive index $\tilde{n}=n_{\text{Re}}+in_{\text{Im}}$, which has a close correspondence with complex dielectric constant $\tilde{\varepsilon}=\varepsilon_{\text{Re}}+i\varepsilon_{\text{Im}}$ of $\tilde{\varepsilon}=\tilde{n}^2$. Therefore,

$$n_{\text{Re}}=\sqrt{\left(\varepsilon_{\text{Re}}+\sqrt{\varepsilon_{\text{Re}}^2+\varepsilon_{\text{Im}}^2}\right)\Big/2} \tag{9}$$

$$n_{\text{Im}}=\sqrt{\left(-\varepsilon_{\text{Re}}+\sqrt{\varepsilon_{\text{Re}}^2+\varepsilon_{\text{Im}}^2}\right)\Big/2} \tag{10}$$

for a given carriers density N, the complex dielectric constant can be expressed, by using Drude model, as [29]

$$\tilde{\varepsilon}=\varepsilon_\infty-\frac{\omega_p^2}{\omega^2+i\Gamma\omega}=\varepsilon_\infty-\frac{\omega_{p,e}^2}{\omega^2+i\Gamma_e\omega}-\frac{\omega_{p,h}^2}{\omega^2+i\Gamma_h\omega} \tag{11}$$

where ε_∞ is the background dielectric constant, the subscripts e and h refer to electron and hole, respectively, and $\Gamma_e=q/m_e\mu_e$ and $\Gamma_h=q/m_h\mu_h$ are the electron and hole damping rates, respectively. q is an electric charge, $m_{e/h}$ and $\mu_{e/h}$ are the effective mass and mobility of carriers, respectively. The real and imaginary parts of the complex dielectric constant can be given as

$$\varepsilon_{\mathrm{Re}} = \varepsilon_{\infty} - \frac{Nq^2\mu_e^2}{\left(m_e^2\mu_e^2\omega^2 + q^2\right)\varepsilon_0} - \frac{Nq^2\mu_h^2}{\left(m_h^2\mu_h^2\omega^2 + q^2\right)\varepsilon_0} \tag{12}$$

$$\varepsilon_{\mathrm{Im}} = \frac{Nq^3\mu_e}{\left(m_e^2\mu_e^2\omega^3 + \omega q^2\right)\varepsilon_0} + \frac{Nq^3\mu_h}{\left(m_h^2\mu_h^2\omega^3 + \omega q^2\right)\varepsilon_0} \tag{13}$$

with ε_0 denoting the permittivity of vacuum.

C. Transmission/reflection formulation

Obviously, the complex refractive index of Si wafer under illumination is varied with *z*. The transmission/reflection of THz waves through such substrate can be calculated by Fresnel transfer matrix, which treats the inhomogeneous medium as a multilayer structure composed of *m* homogenous thin parallel layers with an identical thickness of Δz. The relevant complex refractive index $\tilde{n}_j$ and characteristic matrix $\vec{M}_j$ for the *j*th layer are as eqs. (14) and (15), respectively [30],

$$\tilde{n}_j = \tilde{n}\left(z = jh/m\right) \tag{14}$$

$$\vec{M}_j = \begin{bmatrix} \cos\tilde{\delta}_j & -\dfrac{i\sin\tilde{\delta}_j}{\tilde{\eta}_j} \\ -i\tilde{\eta}_j\sin\tilde{\delta}_j & \cos\tilde{\delta}_j \end{bmatrix} \tag{15}$$

where $\tilde{\delta}_j$ and $\tilde{\eta}_j$ are two characteristic parameters, for a normally incident THz wave, which are defined by

$$\tilde{\delta}_j = \frac{2\pi}{\lambda_0}\tilde{n}_j\Delta z \tag{16}$$

$$\tilde{\eta}_j = \sqrt{\varepsilon_0/\mu_0}\,\tilde{n}_j \tag{17}$$

where λ_0 and μ_0 are the wavelength and permeability of vacuum. The characteristic matrix of the inhomogeneous medium is then given by

$$\vec{M} = \prod_{j=1}^{m}\vec{M}_j = \begin{bmatrix} \tilde{A} & \tilde{B} \\ \tilde{C} & \tilde{D} \end{bmatrix}. \tag{18}$$

The reflection and transmission coefficients of $\tilde{r}$ and $\tilde{t}$ are then derived as

$$\tilde{r} = \frac{(\tilde{A} + \tilde{B}\tilde{\eta}_{m+1})\tilde{\eta}_0 - (\tilde{C} + \tilde{D}\tilde{\eta}_{m+1})}{(\tilde{A} + \tilde{B}\tilde{\eta}_{m+1})\tilde{\eta}_0 + (\tilde{C} + \tilde{D}\tilde{\eta}_{m+1})} \tag{19}$$

$$\tilde{t} = \frac{2\tilde{\eta}_0}{(\tilde{A} + \tilde{B}\tilde{\eta}_{m+1})\tilde{\eta}_0 + (\tilde{C} + \tilde{D}\tilde{\eta}_{m+1})}. \tag{20}$$

Accordingly, the reflectivity and transmittivity are given by

$$R = \left|\tilde{r}\right|^2, \quad T = \left(\tilde{\eta}_{m+1}/\tilde{\eta}_0\right)\left|\tilde{t}\right|^2. \tag{21}$$

In brief, the effective photoexcitation on Si leads to a rapid change of free carriers density as well as refractive index. The resultant refractive index variation contributes to the pronounced changes of THz transmission and reflection. The above theory not only provides a guideline to design or optimize a modulation system beforehand for desirable modulation performance including transmission, modulation depth and lateral resolution [25], but also can be used to analyze carriers dynamics in photo-excited Si through the measured THz time-domain spectroscopy (THZ-TDS) [29].

3. Functional Implementation in THz Manipulation

Although pulsed illumination was applied in the beginning, it is not required but alternative on account of longer carrier lifetime of Si which could allow high-concentration excess carries for THz radiation modulation under low-power continuous wave (CW) excitation, making such optically-manipulated scheme more cost-effective and pow-efficient [31]. Examples are experimental demonstration in Ref. [32] and theoretical simulation in Ref. [25]. Alius and Dodel applied 1060 *nm* CW laser to high-resistivity Si wafer, realizing a maximum intensity modulation of 70%. Both of phase- and frequency-modulation were achieved when two such illumination sources were in use [32]. Kannegulla *et al*. directly deduced the analytical express for carriers density when a CW laser is applied, and also theoretically discussed the physical parameters' influence on the THz modulation, including the substrate thickness, THz frequency, optical illumination width and wavelength [25]. This kind of scheme could realize high-performance (e.g., high modulation efficiency, large modulation depth, fast modulation speed) THz modulation in a simple, cost-effective manner. Not merely does such optical modulation show unique superiority encompassing structural simplicity, economic and flexible fabrication, and wide-range frequency modulation over these metamaterials-based counterparts. But also, various extraordinary manipulation of THz radiation, such as amplitude, frequency, phase, and polarization has been implemented when cooperated with different photopatterned illumination, so did THz beam steering, focusing, filtering, imaging, encoding information on THz waves, etc.

Early to 1996, Brand examined the diffraction by different photo-induced plasma patterns, for the first time, involving several varieties of slits and Fresnel zone plates [33], where, however, most of the beam proceeded in the straight-through direction, only a small fraction was diffracted to the sides. Then, he found most of the reflected radiation would be diffracted into the adjacent interference maxima when a pre-designed cutout mask, which consisted of periodic clear and opaque regions with equal width, was aligned between the optical illumination and Si wafer [34]. This mask projected a grating pattern and thus generated a diffraction grating onto Si wafer. The incident THz radiation was interacted with photo-induced grating and diffracted following Fraunhofer diffraction principle. Thus the direction of reflected beam could be tuned by varying the period of the projected pattern. Wire gratings, as a textbook example, have been widely investigated.

Then derivative grating patterns were adopted by Okada *et al*. for frequency tuning [35, 36]. Combining with a liquid-crystal spatial light modulator (SLM), one-dimensional corrugations (wire-grating patterns), periodically constituted by a broader transparent region and a narrower photoinduced wire, were formed at the surface of a silicon prism by a prepatterned 800 *nm* pulse [35]. They confirmed that the photopatterned structure possessed metallic properties and a characteristic minimum at 0.53 *THz* was observed due to the excitation of surface waves. A line grating patterned at the same surface with uniform fringes also come to an identical consequence [36]. A sharp minimum at lower frequency was observed and the frequency of the characteristic sharp minimum red-shifted with increased period of grating patterns, as shown in Figure 1. A same trend was also obtained for corresponding 2-dimensional square array structure, and each square occupied half a period, once the period kept unchanged. Such uniform periodical rectangular patterns enable real-time, wide-range frequency modulation of THz radiation just by tuning the photogenerated structural periodicity without any microfabrication process.

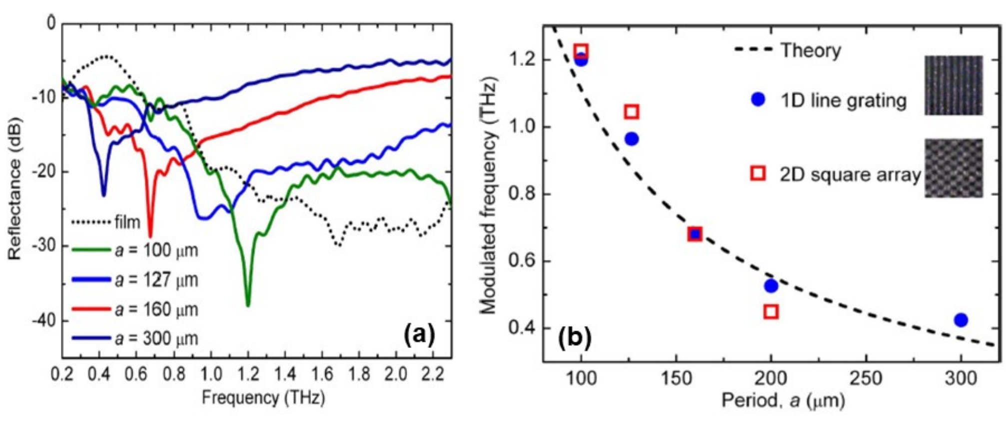

Fig. 1 (a) Modulation performance of photo-designed THz devices as a function of the period of the photo-induced LG. (b) Dependence of spectral minimum frequency on structural periodicity in photo-designed THz devices. [36]

In [37], Cheng and Liu systematically studied several representative types of transmitted THz waves modulations under various photo-excited patterns. These patterns were generated and programmatically reconfigured by a digital light processing (DLP) projector, by which the patterns could be modified and reconfigured optically in a high speed. The experimental setup and modulation types are depicted in Figure 2. With the gray scale varying from bottom to top, the photoexcitation intensity increased and the transmitted THz power reduced, THz intensity modulation was implemented for the illumination patterns in the left column. As for the wire-grid patterns, the reconfigurable THz quasi-optical component shown in Figure 2 (a) acted as a photo-induced polarizer. The polarization angle was tuned by generating rotated images using DLP. Such THz waveform polarizer with subcycle switch-on time was also demonstrated in [38], in which the wire grating was produced by using a shadow mask to shape transverse beam profile of irradiating laser. In addition, chiral patterned photoexcitation, gammadion patterns for instance presented in Figure 3, was also employed to control THz polarization [39]. The resultant polarization rotation was sensitive to the patterns' handedness, with its angle increased with the excitation density and spectra shifted to higher frequencies as the periodicities decreased. These two patterns provide alternative avenues to rotate THz polarization, suggesting that we can design the spectra of the polarization rotation.

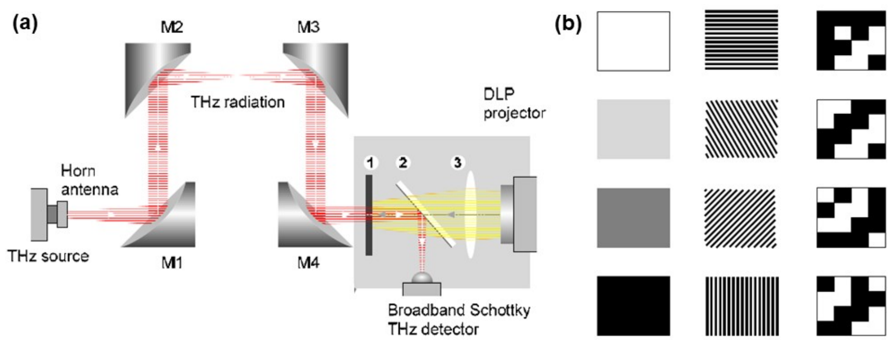

Fig. 2 (a) Experimental setup for THz modulation where 1 represents the semi-insulating Si wafer, 2 is the ITO-coated glass and 3 is the prejection lens. (b) Modulation types: uniform light with different gray scales (left), linear wire grids with varied orientations (middle) and a 4×4 reconfigurable aperture array (right). [38]

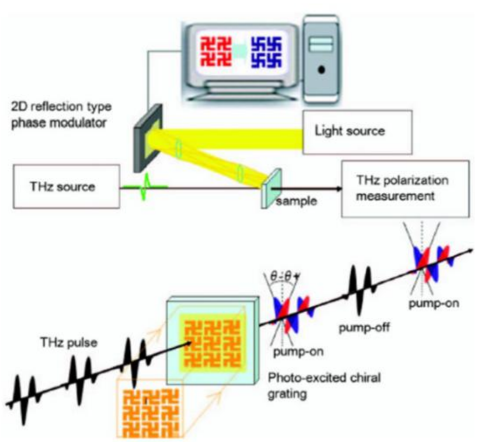

Fig. 3 Schematic of the experimental setup by using 2-dimensional reflection type phase modulator to produce chiral patterned photocarrier distribution. [39]

Except for using a prepatterned radiation, the interference of two titled plane waves is also a valid approach to produce grating pattern on the Si wafer. Rizza *et al*. theoretically investigated the THz dielectric response through a Si slab with such interference pattern [40]. The numerically evaluated results, indicated the interference-induced optical response, could be tailored by varying the photo-generated grating and it ranged from birefringent to hyperbolic to anisotropic negative dielectric while free of microfabrication. But unfortunately, so far there are no reports on the experimental achievements.

In [36], Okada *et al*. verified the feasibility of frequency modulation in reflection by the virtual grating structure formed on Si wafer. And comparable conclusion was made by Busch *et al*. that an increase in line densities, i.e. a decrease in grating period, shifted the peak of penetrated THz signal towards higher frequencies [41]. They also presented a new finding that such technique allowed for an optically controlled beam steering meanwhile. But the tunability of steering is limited compared with those carried out by photo-induced Fresnel zone plate (PI-FZP) [42-44]. Under the wave-front spatial encoding of PI-FZP, both THz beam steering and forming were executed simultaneously. To demonstrate the joint functionalities of beam steering and forming, representative PI-FZP patterns were mapped as shown in Figure 4 (a). The relevant 2-dimensional THz beam profiles in Figure 4 (b)-(e) were measured by these situation sequentially that without PI-FZP, with a PI-FZP of 70 *nm* focal length and 0°, with a PI-FZP of 50 *nm* focal length and 0° and with a PI-FZP of 50 *mm* focal length and 6° steering along 135° direction. Evidently, the use of programmable PI-FZP allowed for progressively more focused beams and also offset from the center as expected but no need for any circuit fabrication or patterning on Si wafer as well as modifying the physical arrangement of the experimental setup. Such dynamically adjustable THz beam steering and forming make it more practical and in demand in adaptive THz wireless communications.

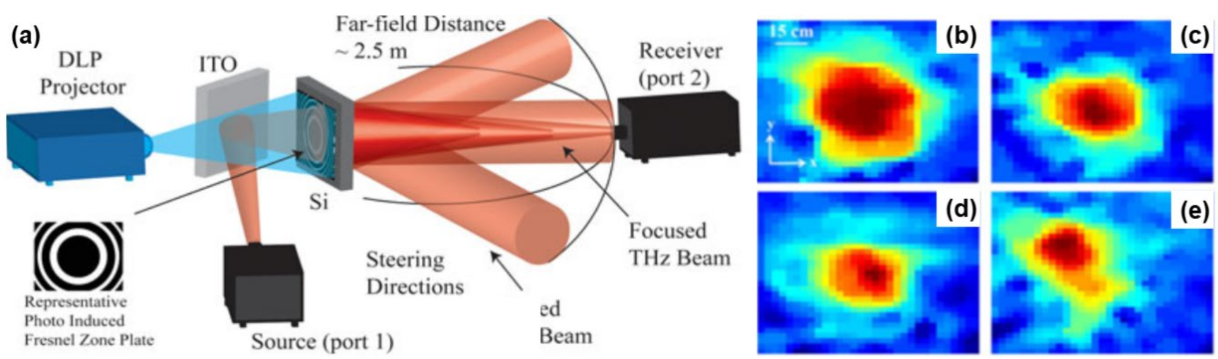

Fig. 4 (a) Experimental setup for transmission, beam steering and forming using PI-PZP. (b)-(e) Measured 2-dimensional radiation intensities showing the THz beam profile for different PI-FZP patterns. [44]

Another strategy of THz wave-front encoding is the utilization of spatial THz modulator (STM) to produce special THz beam based on the computer generated holography [45], whose prototype is exhibited in Figure 5. The required pattern of photo-generated carriers was produced via using a modulated control beam by a conventional SLM to illuminate the surface of a Si wafer. Thus the governed transmission of the THz beam by the density of carriers led to independent modulation of transparency at different positions of the Si wafer. Projected a THz computer generated hologram on the Si wafer, a THz vortex beam with a special phase and amplitude distribution was generated. Such route to encode information in a wave front has paved a new avenue for THz imaging, THz information processing and THz communications.

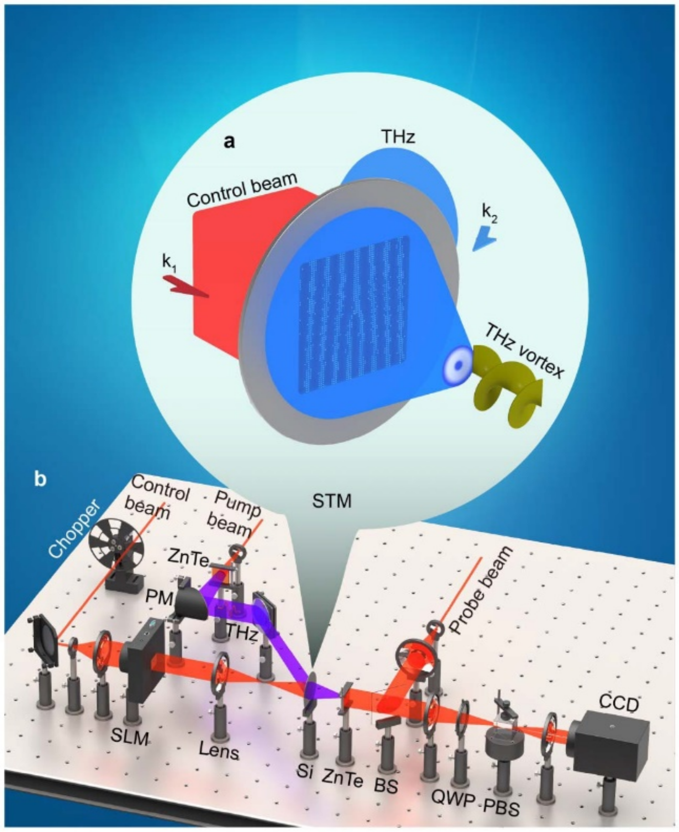

Fig. 5 Prototype and experimental configuration of STM. [45]

Except for these functional elements listed above, tunable THz filters were also designed by an optically gating Si wafer combined with two blazed gratings [46]. As shown in Figure 6 (a), THz radiation diffracting from the blazed grating was focused depending on its angle of incidence at different spatial positions, resulting in spectrally resolved, spatially separated focus points. The light induced absorption in this illuminated spot led to spectral notches. For example, frequency-filtering at 420 *GHz* and 840 *GHz* is shown in Figure 6 (b), where two accessible spectral regions are corresponding to the first and second orders of grating diffraction. In combination with such spatially separated spectrum at the intermediate focus, arbitrary frequencies of THz radiation could be blocked with a customized diffraction grating on the basis of the required filter parameters.

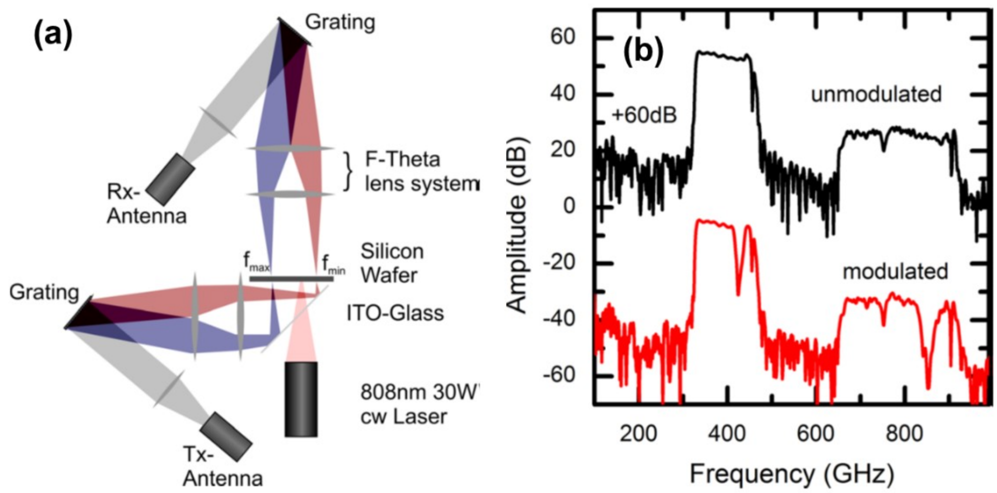

Fig. 6 (a) Experimental setup. (b) THz radiation spectrum of the transmitted first and second orders of diffraction without and with modulation. [46]

4. Performance-Enhanced Photo-Excited Si-Based THz Spatial Modulators

Since this kind of photo-excited Si-based THz spatial modulators has such numerous potential applications, they have been investigated intensively. However devices to control the THz radiation are still rather scarce and generally inefficient. The photoconductivity of standard Si samples tends to saturate, resulting in limited efficiency of most Si-based photomodulators. This necessitates high-power laser sources to achieve significant modulation, which limits the applications of THz systems outside of research laboratories. As such, in recent years, a myriad of coatings such as organic overlayers [47-49], phase-transition materials [50], 2D materials [51-53] and surface-passivation films [54] have been deposited to boost photomodulation by enhancing the light matter interaction. Despite significant improvements have been realized in THz modulation efficiency, the inherent bottlenecks of Si-based photoconductive materials themselves are still being encountered, for example, the high reflection for both the excitation laser and THz radiation at the air-Si interface. Due to the abrupt transition in the refractive index between the surface of air and bare-Si, the resultant reflectivity is as high as 35%~55% across a broad wavelength range of 400~1000 *nm* and ~40% for THz waves. Such high reflectivity not only cripples the modulation efficiency, but also introduces disturbance or noise into the quasi-optical THz system, which greatly limits the achievable tenability and versatility of Si-based STMs. To overcome such deficiencies, our group proposed two different all-optical spatial STMs based on nano- or micro-structuring the Si surface [55, 56].

In our first design, silicon nanotip (SiNT) array was utilized as antireflection layers for THz wave for the first time [55]. By adopting a silver-assisted chemical etch, numerous tapered nanowires were fabricated on the Si wafer. These nanowires have a diameter ranging from 200 *nm* and 350 *nm*. And more importantly they are slightly bundled, approximately perpendicular to the surface, which leaves parts of Si substrate expose to air. The typical SEM image and the schematic of this SiNT-based STM and are shown in Figure 7 (a) and (c), respectively. With such a nano-textured surface, significantly increased transmittance as high as 90% of THz wave was observed and this improvement is strongly dependent with length of nanowires, as shown in Figure 7 (b). Consequently a low-loss and spectrally broadband optical-driven THz modulator was implemented. Moreover, this SiNT array also avails to light harvesting, contributing to a 2~3 times larger modulation efficiency compared with these bare-Si ones.

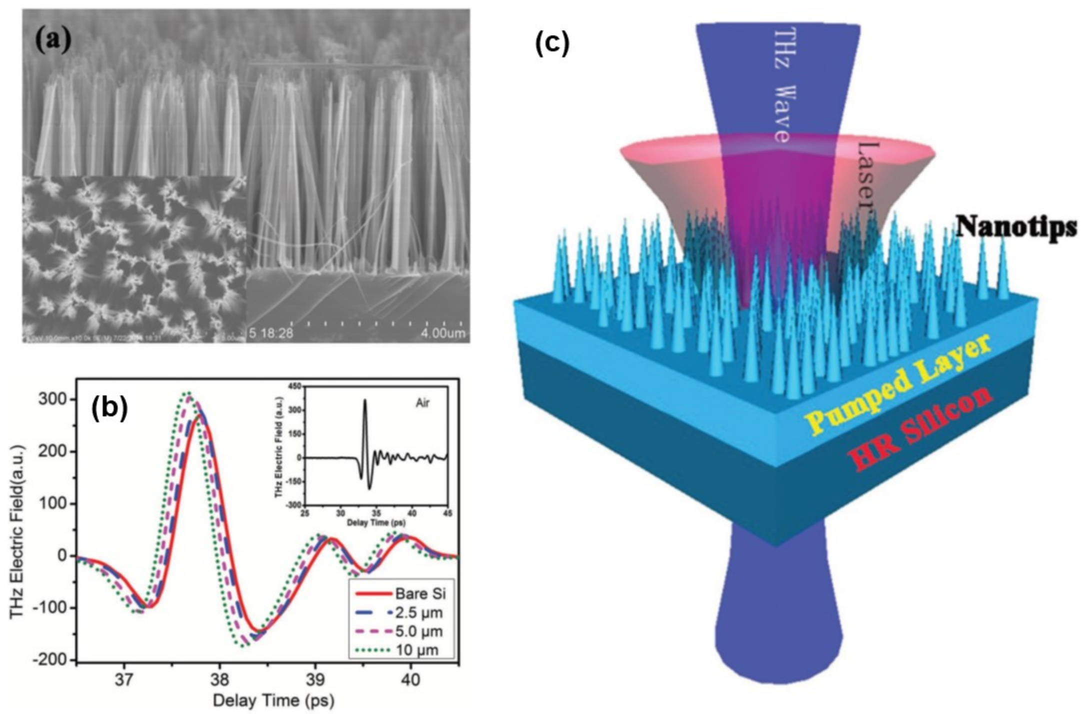

Fig. 7 (a) Cross-sectional SEM image of the SiNT fabricated on the bare-Si substrate and the inset is the top-view image. (b) Prototype and spatial configuration of the SiNT-based STM. (c) The THz time-domain spectrum of the bare Si wafer and SiNT samples with different length. [55]

However this performance-enhanced SiNT-based STM requires a rigorous and subtle balance between the tip shape, wire length and filling ratio but it can only realize a limited improved modulation depth (MD) of 75%. To find a more practicable scheme, an easier anisotropic wet chemical etching technique was adopted [56]. By utilizing the anisotropic response of Si to KOH, pyramid-resembled microstructures were produced on the Si surface, as the SEM image shows in Figure 8 (a). These pyramids are all in a diverse size roughly ranging from 2 *μm* to 10 *μm*, randomly distributed, closely compacted and even partially embedded with each other. This special structure lead to a 1.6-*times* expanded active area for spatial THz modulation as well as 1.4~2-*times* enhanced light harvesting. Although no THz transmission enhancement was observed, this micropyramid array (MPA) based STM achieved a remarkable increase in modulation efficiency, as large as 93.8% under 638 *nm* laser with a low power density of 1 W/cm^2. Furthermore, comparing with bare-Si, this Si-MPA based STM exhibited a reversal relation to laser wavelength, where the modulation efficiency increased with the decrease of illumination wavelength. This different wavelength dependence renders the Si-MPA a superior candidate to constructing a fast THz imager with digital light processing projector (DLP). As a proof of concept, precise THz beam mapping and fast real-time imaging with 225 *pixels* were demonstrated [56]. Very recently, we further realized an enhanced photomodulation efficiency under low illumination density by microtexturing and passivating the Si surface, where as high as 91% MD was obtained at only 0.53 W/cm^2 photodoping [57]. It is demonstrated that this enhancement in efficiency is mainly contributed by the effect of passivation. When a surface is well passivated, the surface recombination of photo-induced carriers is decreased, carrier lifetime is lengthened, and the carrier density in Si is increased, thereby the efficiency is improved. This result also gives a more general explanation to the enhancement by cooperating with various heterogeneous films [47-53], all of which are possibly ascribed to surface passivation including chemical passivation and field-effect passivation. Moreover, the periodically aligned pyramids formed by microstructuring resembled as a mesa array. This array could significantly suppress the lateral diffusion induced by longer diffusion and break the trade-off between resolution and MD.

All of these designs demonstrate that nano- or micro-textured surfaces of Si wafers benefit to decrease the reflection of THz radiation and enhance the light harvesting. But to be unsatisfied, none of the proposed schemes can switch on/off THz radiation and simultaneously increase the transmission of THz radiation. Seeking a new design to achieve these two goals in a simple way will be one of focuses for the future research.

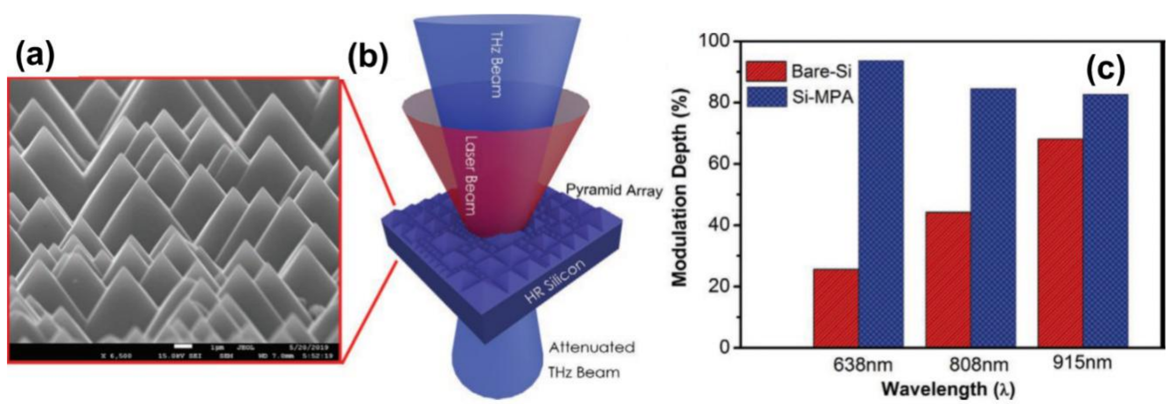

Fig. 8 (a) SEM image of the micropyramid arrays fabricated on the bare-Si substrate. (b) Schematic of Si-MPA-based all-optical THz modulator. (c) Summarized MD under different optical wavelengths with power density of 1 W/cm^2. [56]

5. Outlook

Even though considerable progress has been realized in high-performance STMs, they mainly concentrate on enhancing the modulation efficiency. While modulation speed, as another critical factor in THz imaging and communications systems, is merely investigated for all-optical Si-based STMs. In such optical pumping configurations, the concentration of photo-induced carriers increases with increasing pump power up until saturation, where the carrier recombination rate becomes the determining factor for modulation speed. However, the modulation depth mainly depends on the accumulation of carriers while the modulation speed is determined by the carrier lifetime. Thus there must be a trade-off. Designing a new high-speed and high efficient structure for THz modulation is in an urgent need for actual scenarios. Moreover, the current state-of-the-art THz functional devices are mainly on the basis of bare Si substrate. Its inherent deficiencies include high reflection, limited efficiency and speed render, and its versatility and multifunctionality remain underexploited. Further research with performance-enhanced STMs is also of significance, especially cooperated with other advanced technologies such as coding metasurface.

Funding

Science Challenge Project (TZ2018003); National Natural Science Foundation of China (61831012); International Science and Technology Cooperation Programme (2015DFR50870); Sichuan Province Science and Technology Support Program (2021JDTD0026).

Reference

[1] Y. S. Lee, *Principles of Terahertz Science and Technology*, Springer Science & Business Media, (2009).

[2] H. J. Song and T. Nagatsuma, *Handbook of Terahertz Technologies: Devices and Applications*, Pan Stanford, (2015).

[3] D. Saeedkia, *Handbook of Terahertz Technology for Imaging, Sensing and Communications*, Elsevier, (2013).

[4] M. Tonouchi, “Cutting-edge terahertz technology,” *Nature Photonics*, 1, 97-105 (2007).

[5] P. H. Siegel, “Terahertz technology,” *IEEE Transactions on microwave theory and techniques*, 50(3), 910-928 (2002)

[6] B. Zhu and Z. Han, “Enhanced terahertz fingerprint detection beyond refractive index sensing in a periodic silicon waveguide cavity,” *Journal of Electronic Science and Technology*, 16(2), 105-109 (2018)

[7] P. Hillger, J. Grzyb, R. Jain, *et al.*, “Terahertz imaging and sensing applications with silicon-based technologies,” *IEEE Transactions on Terahertz Science and Technology*, 9(1), 1-19 (2018).

[8] G. Scalari, C. Walther, M. Fischer, *et al.*, "THz and sub-THz quantum cascade lasers," *Laser Photonics Review*, 3, 45-66 (2009).

[9] M. Rahm, J. S. Li, and W. J. Padilla, "THz wave modulators: a brief review on different modulation techniques," *Journal of Infrared, Millimeter, and Terahertz Waves*, 34(1), 1-27 (2013).

[10] L. J. Liang, Z. Zhang, X. Yan, *et al.*, "Broadband terahertz transmission modulation based on hybrid graphene-metal metamaterial," *Journal of Electronic Science and Technology*, 16(2), 98-104 (2018).

[11] Y. Bai, T. Bu, K. Chen, *et al.*, "Review about the optical-controlled terahertz waves modulator," *Applied Spectroscopy Reviews*, 50(9), 707-727 (2015).

[12] L. Fekete, F. Kadlec, P. Kuzel, et al., "Ultrafast opto-terahertz photonic crystal modulator," *Optics Letters*, 32(6), 680-682 (2007).

[13] H. T. Chen, W. J. Padilla, M. J. Cich, *et al.*, "A metamaterial solid-state terahertz phase modulator," *Nature Photonics*, 3(3), 148-151 (2009).

[14] J. S. Li, "Terahertz wave modulator based on optically controllable metamaterial," *Optics and Laser Technology*, 43(1), 102-105 (2011).

[15] Y. P. Li, D. N. Zhang, R. T. Jia, *et al.*, "Mechanism and optimization of a graphene/silicon hybrid diode terahertz modulator". *ACS Applied Electronic Materials*, 2, 1953-1959 (2020).

[16] D. Shrekenhamer, C. M. Watts, and W. J. Padilla, "Terahertz single pixel imaging with an optically controlled dynamic spatial light modulator," *Optics Express*, 21(10), 12507 (2013).

[17] D. H. Auston and C. V. Shank, "Picosecond ellipsometry of transient electron-hole plasmas in germanium," *Physical Review Letters*, 32(20), 1120-1123 (1974).

[18] A. J. Alcock, P. B. Corkum, and D. J. James, "A fast scalable switching technique for high-power CO_2 laser radiation," *Applied Physics Letters*, 27(12), 680 (1975).

[19] S. A. Jamison, A. V. Nurmikko, and H. J. Gerritsen, "Fast transient spectroscopy of the free-carrier plasma edge in Ge," *Applied Physics Letters*, 29(10), 640-643 (1976).

[20] H. Salzmann, T. Vogel, and G. Dodel, "Subnanosecond optical switching of far infrared radiation," *Optics Communications*, 47(5), 340-342 (1983).

[21] L. Fekete, J. Y. Hlinka, E. Kadlec, *et al.*, "Active optical control of the terahertz reflectivity of high-resistivity semiconductors," *Optics Letters*, 30(15), 1992-1994 (2005).

[22] T. Nozokido, H. Minamide, and K. Mizuno, "Modulation of submillimeter wave radiation by laser-produced free carriers in semiconductors," *Electronics & Communications in Japan*, 80(6), 1-9 (2015).

[23] T. Vogel, G. Dodel, E. Holzhauer, *et al.*, "High-speed switching of far-infrared radiation by photoionization in a semiconductor," *Applied Optics*, 31(3), 329-337 (1992).

[24] T. E. Wilson, "Modeling the high-speed switching of far-infrared radiation by photoionization in a semiconductor," *Physical Review B*, 59(20), 12996-13002 (1999).

[25] A. Kannegulla, M. I. B. Shams, L. Liu, *et al*., "Photo-induced spatial modulation of THz waves: opportunities and limitations," *Optics Express*, 23(25), 32098-32112 (2015).

[26] P. Jonsson, H. Bleichner, M. Isberg, *et al*., "The ambipolar Auger coefficient: Measured temperature dependence in electron irradiated and highly injected n-type silicon," *Journal of Applied Physics*, 81(5), 2256-2262 (1997).

[27] J. Linnros and V. Grivickas, "Carrier-diffusion measurements in silicon with a Fourier-transient-grating method," *Physical Review B Condensed Matter*, 50(23), 16943 (1994).

[28] H. M. Driel "Kinetics of high-density plasmas generated in Si by 1.06- and 0.53- microm picosecond laser pulses,". *Physical Review B Condensed Matter*, 35(15), 8166 (1987).

[29] R. Ulbricht, E. Hendry, J. Shan, *et al*., "Carrier dynamics in semiconductors studied with time-resolved terahertz spectroscopy," *Reviews of Modern Physics*, 83(2), 543-586 (2011).

[30] B. E. A. Saleh and M. C. Teich, *Fundamentals of Photonics*, 2nd ed. New York: Wiley (2007).

[31] G. Georgiou, H. K. Tyagi, P. Mulder, *et al*., "Photo-generated THz antennas," *Scientific Reports*, 4(1), 3584 (2014)

[32] H. Alius and G. Dodel G, "Amplitude-, phase-, and frequency modulation of far-infrared radiation by optical excitation of silicon," *Infrared Physics*, 32, 1-11 (1991).

[33] G. F. Brand, "Diffraction of millimeter waves by projecting a shadow pattern onto a semiconductor," *International Journal of Infrared and Millimeter Waves*, 17(7), 1253-1262 (1996).

[34] G. F. Brand, "Remote millimeter-wave beam control by the illumination of a semiconductor," *IEEE Transactions on Microwave Theory and Techniques*, 48(5), 855-857 (2000).

[35] T. Okada, K. Ooi, Y. Nakata, *et al.*, "Direct creation of a photoinduced metallic structure and its optical properties in the terahertz frequency region," *Optics Letters*, 35(10), 1719 (2010).

[36] T. Okada and K. Tanaka, "Photo-designed terahertz devices," *Scientific Reports*, 1(10), 121 (2011)

[37] L. J. Cheng and L. Liu, "Optical modulation of continuous terahertz waves towards cost-effective reconfigurable quasi-optical terahertz components," *Optics Express*, 21(23), 28657-28667 (2013).

[38] N. Kamaraju, A. Rubano, L. Jian, *et al*., "Subcycle control of terahertz waveform polarization using all-optically induced transient metamaterials," *Light: Science & Applications*, 3(2), e155 (2014).

[39] N. Kanda, K. Konishi, and M. Kuwata-Gonokami, "All-photoinduced terahertz optical activity," *Optics Letters*, 39(11), 3274-3277 (2014).

[40] C. Rizza, A. Ciattoni, L. Columbo, *et al*., "Terahertz optically tunable dielectric metamaterials without microfabrication," *Optics letters*, 38(8), 1307-1309 (2013).

[41] S. Busch, B. Scherger, M. Scheller, *et al.*, “Optically controlled terahertz beam steering and imaging,” *Optics Letters*, 37(8), 1391-1393 (2012).

[42] X. Wang, Z. Xie, W. Sun, *et al*., “Focusing and imaging of a virtual all-optical tunable terahertz Fresnel zone plate,” *Optics Letters*, 38(22), 4731-4734 (2013).

[43] M. I. B. Shams, Z. Jiang, J. Qayyum, *et al*., “A terahertz reconfigurable photo-induced fresnel-zone-plate antenna for dynamic two-dimensional beam steering and forming,” in *2015 IEEE MTT-S International Microwave Symposium*, (2015).

[44] M. I. B. Shams, Z. Jiang, S. M. Rahman, *et al*., “A 740-GHz dynamic two-dimensional beam-steering and forming antenna based on photo-induced reconfigurable Fresnel zone plates,” *IEEE Transactions on Terahertz Science and Technology*, 7(3), 310-319 (2017).

[45] Z. Xie, X. Wang, J. Ye, *et al*., “Spatial terahertz modulator,” *Scientific Reports*, 3, 3347 (2013).

[46] S. F. Busch, S. Schumann, C. Jansen, et al., “Optically gated tunable terahertz filters,” *Applied Physics Letters*, 10, 261109 (2012).

[47] M. S. Song, C. Kang, C. S. Kee, *et al*., “Trilayer hybrid structures for highly efficient THz modulation,” *Optics express*, 26(19), 25315-25321 (2018).

[48] W. Liu, F. Fan, S. Xu, *et al*., “Terahertz wave modulation enhanced by laser processed PVA film on Si substrate,” *Scientific Reports*, 8(1), 8304:1-8 (2018).

[49] J. S. Li, S. H. Li, and L. Zhang, “Terahertz modulator using 4-N,N-dimethylamino-4′-N′-methyl-stilbazolium tosylate (DAST)/Si hybrid structure,” *IEEE Photonics Journal*, 10(2), 5900306 (2018).

[50] F. Hu, H. Wang, T. Li, *et al*., “Photo-induced high modulation depth terahertz modulator based on VO_x-Si-VO_x hybrid structure,” *Journal of Physics D: Applied Physics*, 52(17), 175103 (2019).

[51] D. S. Yang, J. Tian, and X. A. Cheng, “Optically controlled terahertz modulator by liquid-exfoliated multilayer WS_2 nanosheets,” *Optics Express*, 25(14), 16364 (2017).

[52] Q. Li, Z. Tian, X. Zhang, *et al*., “Active graphene-silicon hybrid diode for terahertz waves,” *Nature Communications*, 6, 7082 (2015).

[53] S. Chen, F. Fan, Y. Miao, *et al*., “Ultrasensitive terahertz modulation by silicon-grown MoS_2 nanosheets,” *Nanoscale*, 9, 4713-4719 (2016).

[54] I. R. Hooper, N. Grant, L. Barr, *et al*., “High efficiency photomodulators for millimeter wave and THz radiation,” *Scientific Reports*, 9(1), 18304 (2019).

[55] Z. W. Shi, X. X. Cao, Q. Y. Wen, *et al*., “Terahertz modulators based on silicon nanotip array,” *Advanced Optical Materials*, 6(2), 1700620 (2017).

[56] Q. Y. Wen, Y. L. He, Q. H. Yang, *et al.*, “High- performance photo- induced spatial terahertz modulator based on micropyramid silicon array,” *Advanced Materials Technologies*, 5, 1901058 (2020).

[57] Y. L. He, Y. S. Wang, M. Li, et al., "All-optical spatial terahertz modulator with surface-textured and passivated silicon," *Optics Express*, 29(8), 8914-8925 (2021).